The DOI for this manuscript is doi: 10.1175/JCLI-D-14-00389.1

Assessment of sea-ice albedo radiative forcing and feedback over the Northern Hemisphere from 1982 to 2009 using satellite and reanalysis data

Yunfeng Cao[1,2] Shunlin Liang[1,2] Xiaona Chen[1,2] Tao He[2]

[1]State Key Laboratory of Remote Sensing Science, and College of Global Change and Earth System Science, Beijing Normal University

[2]Department of Geographical Sciences, University of Maryland

Corresponding author:Yunfeng Cao, College of Global Change and Earth System Science, Beijing Normal University, No. 19 Xinjiekou Wai Street, Haidian District, Beijing, China, 100875 (willingcao@gmail.com)

Keywords: Arctic, Sea ice, Albedo, Radiative forcing, Trends, Feedback

Abstract

The decreasing surface albedo caused by continously retreating sea ice over Arctic plays a critical role in Arctic warming amplification. However, the quantification of the change in radiative forcing at top of atmosphere (TOA) introduced by the decreasing sea ice albedo and its feedback to the climate remain uncertain. In this study, based on satellite-retrieved long-term surface albedo product CLARA-A1 and radiative kernel method, an estimated 0.20 ± 0.05 W m^{-2} sea ice radiative forcing (SIRF) has decreased in the Northern Hemisphere (NH) owing to the loss of sea ice from 1982 to 2009, yield a sea-ice albedo feedback (SIAF) of 0.25 W m^{-2} K^{-1} for NH and 0.19 W m^{-2} K^{-1} for the entire globe. These results are lower than the estimate from another method directly using the Clouds and the Earth's Energy (CERES) broadband planetary albedo. Further data analysis indicates that kernel method is likely to underestimate the change in all-sky SIRF because all-sky radiative kernels mask too much of the effect of sea ice albedo on the variation of cloudy albedo. By applying an adjustment with CERES-based estimate, the change in all-sky SIRF over NH was corrected to 0.33 ± 0.09 W m^{-2}, corresponding to a SIAF of 0.43 W m^{-2} K^{-1} for NH and 0.31 W m^{-2} K^{-1} for the entire globe. We also determine that relative to satellite surface albedo product, two popular reanalysis products - ERA-Interim and MERRA, severely underestimate the changes in NH SIRF in melt season (May to August) from 1982 to 2009 and the sea ice albedo feedback to warming climate.

1. Introduction

Sea surface albedo in the Arctic Ocean has declined considerably over the past decades (Comiso and Hall 2014; Riihelä et al. 2013a) because of retreating sea ice coverage (Comiso et al. 2008; Kerr 2009; Parkinson and Cavalieri 2012), earlier melt onset (Markus et al. 2009; Stroeve et al. 2014), and decreasing ice thickness (Kwok and Rothrock 2009; Maslanik et al. 2007), which have forced the Arctic Ocean to absorb increasing amounts of solar radiation (Perovich et al. 2007b).

Sea ice albedo feedback (SIAF) has largely enhanced Arctic warming. Some studies suggest that SIAF played a central role in the recent Arctic warming amplification (Crook et al. 2011; Screen and Simmonds 2010; Serreze et al. 2009; Taylor et al. 2013). While other studies argue that compared to the temperature feedbacks (especially the lapse rate feedback), the contribution of SIAF to the Arctic warming amplification is not substantial (Pithan and Mauritsen 2014), or even negligible (Winton 2006). Therefore, a more accurate quantification of the Arctic SIAF is essential for understanding the physical mechanisms of accelerated sea ice loss and assessing the underlying evolution of Arctic warming amplification.

Most previous surface albedo feedback assessments have been based on model simulations (Colman 2003; Colman 2013; Dessler 2013; Pithan and Mauritsen 2014; Taylor et al. 2013; Winton 2006), while estimates through satellite retrievals remain limited. Two recent, typical studies based on satellite retrievals show large differences from one another. Flanner et al. (2011) used a synthesis of calculated sea ice albedo, with sea ice type derived from sea ice concentration and in situ measurements of sea ice albedo, and radiative kernels to estimate the sea ice radiative forcing (SIRF) in the Northern Hemisphere (NH). They found the change in SIRF from 1979 to 2008 was 0.22 (0.15 – 0.32) W m^{-2}, and the corresponding SIAF was 0.28 (0.19 – 0.41) W m^{-2}

K^{-1} based on surface temperature warming of 0.79 K reported by Goddard Institute of Space Studies (GISS) during that period. Pistone et al. (2014) estimated Arctic SIRF (although they didn't use this concept directly) and SIAF from 1979 to 2011 with a combined time series of planetary albedo: For the period from 2000 to 2011, they used the observed planetary albedo from Clouds and Earth's Radiant Energy System (CERES) product; For the period from 1979 to 1999, they used a derived planetary albedo from sea ice concentration. They found the change in SIRF in the NH caused by sea ice loss north of 60°N was 0.43 ± 0.07 W m^{-2}, which was nearly twice as larger as that estimated by Flanner et al. (2011). The results of these two studies differ considerably, despite the fact that both studies used the same method to calculate the change in SIRF (expressed as linear trend multiplied by the time interval) over a similar time period, and the same GISS surface temperature product.

Flanner et al. (2011) also compared their estimated SIAF to a Coupled Model Inter-comparison Project (CMIP3) multi-model based estimate, and indicated that CMIP3 models substantially underestimated the change in NH SIRF because of a systematically slower decline in the simulated sea ice concentration compared to observed rates (Flanner et al. 2011; Stroeve et al. 2007). However, Dessler (2013) estimated the global surface albedo feedbacks using two reanalysis products - ECMWF Interim Re-Analysis (ERA-Interim) and Modern Era Retrospective-Analysis for Research and Applications (MERRA), and compared them to the estimates from general circulation models (GCMs). He found that the global surface albedo feedbacks of 0.28 ± 0.15 W m^{-2} K^{-1} (ERA-Interim) and 0.24 ± 0.15 W m^{-2} K^{-1} (MERRA) are close to the values of 0.3 ± 0.12 W m^{-2} K^{-1} (control runs) and 0.28 ± 0.09 W m^{-2} K^{-1} (A1B) estimated by GCMs. Finally, Dessler (2013) drew a contradictory conclusion to Flanner et al. (2011), that there is no evidence GCMs underestimate surface albedo feedback.

In this study, CLARA-A1, a newly released satellite-retrieved long-term surface albedo product from the Advanced Very High Resolution Radiometer (AVHRR) (Riihelä et al. 2013b) , which is different from the datasets used by Flanner et al. (2011) and Pistone et al. (2014), is used to estimate the change in NH SIRF and SIAF from 1982 to 2009. But, in order to make it comparable, the same GISS surface temperature record (Hansen et al. 2010) and the same linear change calculation method as the two previous studies (Flanner et al. 2011; Pistone et al. 2014) are applied. The disagreement between the previous studies are analyzed and reconciled by adjusting change in all-sky SIRF estimated from kernel method. In addition, we compare the satellite albedo-based estimates to those from ERA-Interim and MERRA reanalysis to evaluate the performance of reanalysis on the assessment of change in NH SIRF and SIAF.

2. Data and Methods

2.1 Data

Surface Albedo: Three monthly surface albedo products from 1982 to 2009 are used: CLARA-A1 satellite retrieved surface albedo product, ERA-Interim and MERRA reanalysis albedo products. The CLARA-A1 product was developed by the European Organization for the Exploitation of Meteorological Satellites (CM SAF) project from AVHRR data with a spatial resolution of 0.25° × 0.25°. A homogenization pre-processing was taken to remove inter-satellite calibration differences in the imagery and make the retrievable albedo data set internally consistent (Riihelä et al. 2013b). The retrieval accuracy for sea ice albedo validated with in situ measurements is approximately 10–15% (Riihelä et al. 2013a; Riihelä et al. 2013b). There are some gaps in the original CLARA surface albedo product around the North Pole in the large solar zenith angle months. Using the seasonal variation from previous studies (Flanner et al. 2011; Pistone et al. 2014) and the value of neighboring month, we filled in the missing pixels, although they did not significantly affect the estimation of SIRF and its changes because of little incoming solar radiation in these regions and months. The ERA-Interim product is the latest global atmospheric reanalysis dataset produced by the European Centre for Medium-Range Weather Forecasts (ECMWF) based on an improvement over the ERA-40 dataset (Dee et al. 2011; Screen and Simmonds 2010). The monthly ERA-Interim sea ice albedo was calculated with the 0.25° × 0.25° clear-sky surface downward and upward shortwave fluxes. The monthly 0.67° × 0.50° MERRA sea ice albedo is produced by NASA's Global Modeling and Assimilation Office (Rienecker et al. 2011).

Radiative flux: The CERES Single Satellite Footprint 1.0° (SSF1deg) TOA observed broadband radiative flux, which is a recommended product for long term climate trend evaluation by the CERES science team and was also successfully used by Pistone et al. (2014) to estimate the Arctic SIRF and SIAF, is introduced for comparison with the kernel method of synthesis of surface albedo and radiative kernels.

Cloud fraction: The CERES SSF 1.0° cloud fraction product, derived using CERES-MODIS cloud retrieval algorithm, from 2000 to 2009 and the CLARA-A1 0.25° cloud fraction, derived from the EUMETSAT Nowcasting Satellite Application Facility NWC SAF cloud-processing package (Karlsson et al. 2013), from 1982 to 2009 are used in adjusting the change in all-sky SIRF estimated by kernel method.

Sea ice extent: The fourth version of the NH EASE-Grid 2.0 Weekly Snow Cover and Sea Ice Extent product, which was gridded to EASE-Grid from Sea Ice Concentrations and derived from Nimbus-7 Scanning Multichannel Microwave Radiometer (SMMR) and Defense Meteorological Satellite Program (DMSP) SSM/I-SSMIS Passive Microwave Data, provided by the National

Snow and Ice Data Center (NSIDC), is used to recognize the maximum sea ice coverage from 1982 to 2009.

Surface temperature: The GISS Gridded Monthly mean 2° × 2° Combined Land–Surface Air and Sea–Surface Water Temperature Anomalies (Hansen et al. 2010) (Land–Ocean Temperature Index, LOTI) is used in the study to calculate the change in surface temperature in NH and the entire globe from 1982 to 2009.

2.2 Methods

Following the radiative kernel method, the time (t) dependent SIRF within a region R (here, the NH) of area A and the SIAF can be estimated separately in two steps (Flanner et al. 2011; Qu and Hall 2006):

$$SIRF(t,R) = \frac{1}{A(R)} \int_R I(t,r) \frac{\partial \alpha_p}{\partial \alpha_s}(t,r) \alpha_{csi}(t,r) dA(r) \quad (1),$$

$$SIAF = \frac{\Delta SIRF}{\Delta T_s} \quad (2).$$

As shown in formula (1), the pixel-level SIRF can be calculated in three terms, representing individual contribution or process: $I(t,r)$ is the TOA incoming solar radiation, $\partial \alpha_p / \partial \alpha_s$ represents the change in planetary albedo resulting from a standard perturbation of surface albedo (usually specified as 1%), and α_{csi} is the sea ice surface albedo contrast, calculated as the sea ice surface albedo minus the open ocean water albedo (here, 0.0676). The term $I(t,r)$ together with $\partial \alpha_p / \partial \alpha_s$ forms the radiative kernel, which are usually described as the TOA flux variation with surface albedo change ($\partial F / \partial \alpha$). There is a slight difference in formula (1) from that in the study by Flanner et al. (2011), the albedo products (CLARA, ERA-Interim, and

MERRA) are the ocean surface albedo of both sea ice and open water, so another parameter to characterize the influence of sea ice cover fraction on SIRF is unnecessary.

There are currently three methods to generate the radiative kernels: 1) a physically based regression model that expresses planetary albedo as a function of different contributions, such as surface albedo, cloud cover, and cloud optical thickness (Qu and Hall 2006); 2) an analytical model that expresses planetary albedo as the sum of the contributions of surface and atmosphere, each with an analytical function (Donohoe and Battisti 2011); and 3) a simulated method using an offline radiative transfer code to calculate the change in planetary albedo associated with a unit (1%) perturbation of surface albedo based on climate models (Shell et al. 2008; Soden et al. 2008). It suggested that the simulated method is likely more accurate than the other two methods (Qu and Hall 2013). Two widely used monthly radiative kernels are applied, one generated with the Geophysical Fluid Dynamics Laboratory Atmosphere Model 2 (GFDL AM2), and the other with the National Center for Atmosphere Research Community Atmosphere Model version 3 (NCAR CAM3) (Shell et al. 2008; Soden et al. 2008), to estimate the SIRF separately, and are averaged to obtain mean SIRF.

The TOA shortwave radiative forcing and its changes from 2000 to 2009 are also calculated with CERES SSF planetary albedo and insolation, following the method applied by Pistone et al. (2014). The result is compared with those from the kernel method and used for adjusting the all-sky estimate.

Based on formula (2), SIAF can be calculated as the change in SIRF ($\Delta SIRF$) divided by the change in surface temperature (ΔT_s). Both $\Delta SIRF$ and ΔT_s are calculated as the linear trends multiplied by the time intervals, the uncertainty of the changes are given as the 95% confidence intervals of the fit multiplied by the time intervals. Owing to the onset of polar night, we consider only the months March through September for albedo, and calculate the annual mean (January to December) surface temperature over the globe and the NH.

All variables and the radiative kernels are re-gridded to a spatial resolution of 0.25° × 0.25° in the first step to estimate the SIRF on pixel-level. Then, the SIRF and cloud fraction maps are re-projected to equal area projection, and the maximum sea ice coverage area from 1982 to 2009 in the NH recognized by the EASE-Grid 2.0 Weekly Sea Ice Extent product are applied as a mask to statistically measure the regional average of all of the variables.

3. Results

3.1 Radiative Forcing of Sea Ice Albedo

Based on the surface albedo contrast, radiative kernels and sea ice extension mask, we calculate the multi-year averaged clear-sky and all-sky NH SIRFs with three albedo products (Table 1). All values in Table 1 are calculated as the average of SIRFs estimated using two radiative kernels. Uncertainties are the 95% confidence intervals of the multi-year averaged annual SIRFs, Min and Max are the minimum and maximum values of the SIRF time series.

As seen in Table 1, the all-sky SIRF in NH averaged over 1982–2009 calculated with CLARA is -1.65 ± 0.14 W m^{-2}, which is very similar to that of ERA-Interim, -1.71 ± 0.08 W m^{-2}, and both are larger than that of MERRA, -1.40 ± 0.07 W m^{-2}. The satellite observed SIRF here from CLARA is slightly larger than that given by Flanner et al. (2011) (similar to the upper bound), -1.34 (-0.92 to -1.70 in their Table 1) W m^{-2}. Even for estimates using the same radiative kernels, the all-sky SIRF given by Flanner et al. (2011) is still smaller, about -1.40 (-1.13 to 1.63) W m^{-2}. The difference can be partly attributed to the parameterized sea ice albedo calculation method, which may underestimate the North Pole-centered sea-ice albedo in melt season (Flanner et al. 2011; Perovich et al. 2007a). Additionally, a small portion of the difference could be due to the different time periods used for analysis in these studies. The clear-sky SIRFs are nearly twice that of the all-sky SIRFs for all three products, indicating that the cooling effect of sea ice albedo on the Arctic climate is weakened by cloud overspread.

The seasonal cycles of SIRF for all three products shown in Fig. 1 indicates that both all-sky and clear-sky SIRF occur mainly in spring and early summer, particularly March to June, and peak in May as a result of the large magnitude of pre-melt sea ice albedo and relatively higher insolation. Both satellite-retrieved and reanalysis data can capture the seasonal variation of SIRF, which are very similar to the estimate by Flanner et al. (2011). However, the SIRF estimated with MERRA is smaller than other two products from March to June because of its relatively lower sea ice albedo in this period, which results in the lower multi-year averaged SIRF. The seasonal variation of SIRF also indicates that it is reasonable to use the months from March to September to represent the entire year (Pistone et al. 2014). Based on data analysis, insolation from October through February contributes little (about 4% in total) to the annual averaged incoming radiative flux in the Arctic region.

The spatial distribution of NH SIRF averaged from 1982 to 2009 with CLARA and two other reanalysis datasets are shown in Fig. 2. It demonstrate the annual-mean NH SIRF occurs mainly in the region north of 70°N, which may be due to the longer annual coverage time of ice cover over this area. Therefore, studies focusing on the SIRF and its changes over the region of 60°N–90°N can represent the entire NH to a great extent and are comparable to studies focusing only on 70°N–90°N. As shown in Fig. 2, the annual-mean SIRF at TOA in the Arctic Ocean can be larger than 40 W m^{-2} for all-sky and 60 W m^{-2} for clear-sky. Overall, the magnitude of SIRF estimated with CLARA surface albedo is very similar to that of ERA-Interim, and both are larger than that of MERRA.

3.2 Changes in Sea Ice Albedo Radiative Forcing (ΔSIRF)

The time series of annual-mean (March to September) spatial-mean SIRFs together with the statistical linear changes of SIRFs are shown in Fig. 3, all SIRFs have been averaged over the entire NH. The ΔSIRFs from 1982 to 2009 are calculated as the linear trend of the SIRF time series multiplied by the time intervals. Uncertainties of the changes are calculated as the 95% confidence intervals of the trend multiplied by the time intervals. The all-sky ΔSIRF over the NH with the CLARA albedo product is 0.20 ± 0.05 W m^{-2}, which is equivalent to an energy increase of 0.10 ± 0.03 W m^{-2} over the entire globe. The clear-sky NH ΔSIRF with CLARA albedo is 0.46 ± 0.12 W m^{-2}. Both all-sky and clear-sky NH ΔSIRFs estimated with satellite retrievals are larger (nearly two times) than those of the other two reanalysis products, imply that although satellite retrieved product is not perfect, it's able to capture the change in surface albedo caused sea ice loss. In light of these results and given the conclusions of the previous studies (Dessler 2013; Flanner et al. 2011), we can conclude that both reanalysis datasets and CMIP3 GCMs underestimate the NH ΔSIRF for the last three decades.

The estimated NH ΔSIRF of 0.20 ± 0.05 W m^{-2} with CLARA albedo is very close to the value of 0.22 (0.15 - 0.32) W m^{-2} averaged over 12 all-sky kernel estimates presented by Flanner et al. (2011). Considering the shorter time period (28 years) in this study compared to the previous study (30 years) and the method to calculate ΔSIRF (dependent on time intervals), nearly the same estimate is obtained here as Flanner et al. (2011). However, both estimates are lower than that by Pistone et al. (2014), who estimated the ΔSIRF from 1979 to 2011 to be 0.43 ± 0.07 W m^{-2} with TOA observationally based planetary albedo product.

Fig. 4 shows the monthly NH ΔSIRF from 1982 to 2009, which indicates that the change in NH SIRF occurs primarily in the melt season (May to August), when both the TOA insolation and the change in surface albedo are relatively larger, and peaks in June for both clear-sky and all-sky conditions with the largest ΔSIRF values as 1.36 ± 0.50 W m^{-2} and 0.64 ± 0.25 W m^{-2} respectively. The seasonal variation of ΔSIRF appears similar to the results of Flanner et al. (2011). The large relative uncertainty of all-sky ΔSIRF in July is high likely caused by the high cloud fraction during this period (Karlsson and Svensson 2013). It also shows both ERA-Interim and MERRA significantly underestimate the change in SIRF in the melt season, and consequently the annual averaged ΔSIRF.

The spatial distribution of NH ΔSIRF shown in Fig. 5 indicates that the change in sea ice surface albedo during the last three decades occurred mainly from 70°N–80°N in the Arctic Ocean. Three hot spots- Baffin Bay, North Barents-Kara Sea, and Chukchi Sea, play leading roles in the process of changing SIRF. Both ERA-Interim and MERRA can replicate the main spatial patterns of the ΔSIRF, but are numerically lower than the estimates with the CLARA surface albedo product. It should be noted that even though both reanalysis products underestimate the change in SIRF, the reasons are likely different. For ERA-interim, the negative change in SIRF in the polar region (north of 83°N) and east of Greenland may bring down the total ΔSIRF. While for MERRA, the nearly zero change in SIRF in the polar region (north of 80°N) combined with the lower magnitudes in the margin (70°N–80°N) region may result in the smaller total ΔSIRF. More accurate data assimilation in the polar region (north of 80°N) would greatly improve the quality of reanalysis.

3.3 Sea Ice Albedo Feedback (SIAF)

The changes of annual-mean (January to December) surface air temperature (ΔT_s) from 1982 to 2009 estimated with the GISS surface temperature product are 0.79 ± 0.16 K over the Northern Hemisphere and 0.54 ± 0.12 K over the entire globe (Fig. 6). By combining ΔSIRF and

ΔT_s, the feedback parameter associated with the change in NH sea ice albedo (NH SIAF) can be calculated with formula (2). Table 2 shows the SIAF and the calculated range (low and high bound) for each product (e.g., for the low bound, divide minimum ΔSIRF by maximum ΔT_s and vice versa for the high bound).

As shown in Table 2, the reanalysis-based estimates of global SIAF are 0.09 (0.05–0.17) W m^{-1} K^{-1} for ERA-Interim and 0.07 (0.04–0.13) W m^{-2} K^{-1} for MERRA, which are close to the model-based estimations of 0.10 ± 0.03 W m^{-2} K^{-1} from CMIP3 models and 0.11 ± 0.04 W m^{-2} K^{-1} from CMIP5 models reported in previous studies (Winton 2006; Pistone et al. 2014) within the range of uncertainties. This is consistent with Dessler's (2013) findings. However, both ERA-Interim and MERRA underestimate nearly half of the NH SIAF to the global climate compared to the CLARA satellite-based estimate of 0.19 (0.11–0.30) W m^{-2} K^{-1}. The SIAF for NH is 0.25 (0.16–0.40) W m^{-2} K^{-1}, which is consistent with the Flanner et al. (2011) estimate of 0.28 (0.19 – 0.41) W m^{-2} K^{-1}.

3.4 Adjustment of satellite based all-sky ΔSIRF and SIAF

As indicated above, the estimates of ΔSIRF with CLARA satellite-retrieved long-term time series surface albedo is nearly the same as that of Flanner et al. (2011). However, both all-sky estimates are only half of a recent estimate by Pistone et al. (2014), who used a derived planetary albedo directly. In order to determine the underlying causes of the difference between our estimate and that given by Pistone et al. (2014), the SIRF values estimated with kernel method and the TOA planetary albedo from CERES SSF product during the overlapping period from 2000 to 2009 were analyzed. The data processing for CERES SSF product is based on the same spatial domain (the maximum sea ice coverage area from 1982 to 2009 in the NH), and the same temporal domain (the months from March to September). The regional average statistics are also based on equal area map projection.

As shown in Fig. 7, the clear-sky ΔSIRF from 2000 to 2009 calculated using radiative kernels with CLARA surface albedo is 4.13 ± 1.84 W m^{-2}, slightly lower than CERES SSF observed change in clear-sky TOA reflected shortwave flux of 4.56 ± 1.75 W m^{-2}, which may be due to a small decrease in planetary albedo from increasing water vapor in the Arctic atmosphere (Dessler et al. 2013; Serreze et al. 2012). Pistone et al. (2014) also acknowledge that their estimate is an upper bound because of the decrease of the albedo caused by other factors. This implies that the clear-sky ΔSIRF estimated using the radiative kernels with the satellite albedo is more reliable for it has excluded the influences from other climate variables on the change in clear-sky planetary albedo. However, the all-sky ΔSIRF of 1.81 ± 0.92 W m^{-2} calculated using the radiative kernels is much lower than the change in all-sky TOA reflected shortwave flux (2.85 ± 0.99 W m^{-2}) from CERES SSF products, indicating that the difference between the two methods may lie in the interaction of sea ice albedo and cloud radiation (the response of cloud albedo to the variation of surface sea ice albedo). It has been found that changes in surface sea ice albedo can result in a change in cloud albedo (and thus cloud radiative forcing), even if the cloud properties do not change (Shell et al. 2008). Inspired by this finding, we attempt to determine the causes to the variation of cloudy-sky albedo in Arctic Ocean.

Following the previous study (Pistone et al. 2014), all-sky planetary albedo is related to cloudy-sky planetary albedo, clear-sky planetary albedo and cloud fraction (f_c), as shown in formula (3). In order to estimate the changes of radiative flux, all albedo parameters have been converted to upward shortwave radiative flux (i.e., clear-sky upward SW (SW_{cs}), cloudy-sky upward SW (SW_{cld}), and all-sky upward shortwave flux (SW_{as})) by multiplying the planetary albedo by a TOA climatology insolation.

$$SW_{as} = SW_{cs}\,(1 - f_c) + SW_{cld}\, f_c \;. \qquad (3)$$

If all other terms are known, the TOA SW_{cld} can be calculated with the above equation. Figure 7 (c) shows the calculated SW_{cld} based on the CERES SSF clear-sky, all-sky planetary albedo, TOA solar insolation flux, and the cloud fraction from the CERES–MODIS product. The figure indicates that the cloud reflected shortwave radiative flux decreases significantly. It's clear that most changes in clear-sky planetary albedo are due to the variation of sea ice (and thus sea ice albedo) (Koenigk et al. 2014; Pistone et al. 2014). Therefore, the high correlation between cloudy-sky and clear-sky upward shortwave radiative flux shown in Fig. 7 (d) implies that the decrease of cloudy-sky planetary albedo over the Arctic Ocean is very likely to have arisen from the change in surface sea ice albedo as well, and is unfortunately underestimated by all-sky radiative kernels. The current CAM radiative kernel generated from the CAM5 model masks much less of the sea ice albedo effect on the TOA shortwave radiative flux which may offer a more realistic estimate of Arctic SIRF and its change (Perket et al. 2014). We also analyze the relationship between cloudy-sky planetary albedo and cloud optical thickness, find no significant correlation between them. Based on the analysis above, we adjust the underestimated all-sky ΔSIRF by the kernels method.

Cloud coverage can significantly influence the variation of all-sky planetary albedo. In order to remove the effect of cloud fraction on the variation of SW_{as}, we fix the cloud fraction in the first year (2000) and then recaculate SW_{as} with formula (3) to get an adjusted all-sky upward shortwave radiative flux (SW_{aas}, as shown in Fig. 7(c)). The year 2000 is chosen for fixing the cloud fraction because cloud fraction in this year is 72.2%, nearly the same as the multi-year average, 72.6%, a different cloud fraction would introduce a small uncertainty (about 1%) to the correction factor in formula (4). Afterwards, the change in adjusted all-sky upward SW (ΔSW_{aas}) is 3.30 ± 1.32 W m^{-2}. Based on the radiative kernel method, a time-invariant cloud fraction results in a time-invariant ratio of all-sky ΔSIRF to clear-sky ΔSIRF, which means the ratio of ΔSW_{aas} to ΔSW_{cs} during 2000 to 2009 can be used to correct the underestimated all-sky ΔSIRF from kernel method with formula (4).

$$\Delta SIRF_{aas} = \Delta SIRF_{cs} \frac{\Delta SW_{aas}}{\Delta SW_{cs}} \quad (4)$$

Here, $\Delta SIRF_{cs}$ is the clear-sky ΔSIRF estimated with the radiative kernels, ΔSW_{aas} is the change in adjusted all-sky upward shortwave radiative flux, ΔSW_{cs} is the change in clear-sky upward shortwave radiative flux estimated with CERES SSF products, the ratio of ΔSW_{aas} to ΔSW_{cs} is the correction factor, and $\Delta SIRF_{aas}$ is the corrected all-sky ΔSIRF estimated with kernels. After correction, the all-sky ΔSIRF from 2000 to 2009 is 2.99 W m^{-2}. The annual averaged (March to September) cloud fraction over Arctic Ocean from CLARA product shows no significant change over 1982 to 2009, and the multi-year mean value is about 72.5% (Fig. 8), which is the same as multi-year averaged cloud fraction of 72.6% estimated with the CERES SSF cloud fraction product (Fig. 7 (c)) from 2000 to 2009. This means the all-sky ΔSIRF from 1982 to 2009 can also be corrected directly with formula (4) and the correction factor generated from CERES SSF TOA product during 2000 to 2009. The kenel-based all-sky NH ΔSIRF can be corrected from 0.20 ± 0.05 W m^{-2} to 0.33 ± 0.09 W m^{-2}, which is larger than the lower bound estimate from Flanner et al. (2011), and smaller than the upper bound estimate from Pistone et al.

(2014). Correspondingly, the all-sky SIAF can be adjusted to 0.42 W m^{-2} K^{-1} for the NH and 0.31 W m^{-2} K^{-1} for the entire globe.

4. Discussion

In this study, only the months March through September are considered for the estimation of annual averaged radiative forcing, because the insolation during October through February contributes very little (about 4%, which would lead to a small underestimation for the annual-mean SIRF) to the annual radiative flux in the Arctic region. For the calculated changes in SIRFs during last three decades, the influence from these months is even negligible, because the decrease of sea ice (and thus albedo) happens primarily in the melt season.

When we try to determine if the change in all-sky SIRF estimated with kernel method is underestimated or not, the key issue is which climate varible caused the variation of cloudy-sky planetary albedo. Through data analysis with CERES SSF TOA products, we find, the variations (more than 90%) of cloudy-sky planetary albedo over Arctic Ocean are mainly caused by sea ice loss (and thus decreasing sea ice albedo), while cloud optical thickness has little effect on the change in cloudy-sky albedo. Based on this important finding, we adjusted the change in SIRF estimated using the kernel methods with surface albedo and obtain a more realistic estimate between the lower bound from Flanner et al. (2011) and the upper bound from Pistone et al. (2014). Considering the underestimation of change in all-sky SIRF by kernel method, a more accurate simulation on the response of cloudy-sky planetary albedo to the variation of surface albedo would greatly help improve the simulation of energy budget and the future sea ice loss in Arctic.

5. Conclusions

The role of SIAF in Arctic warming amplification continues to be a debated issue (Graversen et al. 2014; Kumar et al. 2010; Pithan and Mauritsen 2014; Screen and Simmonds 2010). An improved quantification of the SIAF is critical for better understanding of the physical mechanisms of the accelerated Arctic sea ice loss and assessing the underlying future evolution of the Arctic warming amplification. Most previous SIAF assessments were based on model simulations (Colman 2003; Colman 2013; Dessler 2013; Pithan and Mauritsen 2014; Taylor et al. 2013; Winton 2006). Two recent studies used synthesized satellite-observed long-term products, reached significantly different results (Flanner et al. 2011; Pistone et al. 2014). To take advantage of both satellite observation and model simulations, an approach was proposed to estimate the change in SIRF and SIAF to the climate over NH and the entire globe from 1982 to 2009.

Based on the assessment using kernel method with CLARA surface albedo product, the NH all -sky SIRF is estimated as -1.65 ± 0.14 W m^{-2}, and the linear change of all-sky SIRF indicates that 0.20 ± 0.05 W m^{-2} shortwave radiative flux was absorbed by the NH Earth owing to the loss of sea ice within the 28-year period, yield an SIAF of 0.25 W m^{-2} K^{-1} for NH and 0.19 W m^{-2} K^{-1} for the entire globe. This result is the same as the estimate from Flanner et al. (2011) who also used the kernel method, but both are smaller than that reported by Pistone et al. (2014) who estimated the change in SIRF directly using planetary albedo. In order to reconcile the difference between two methods, further data analysis is taken and indicates that although kernel method can separate the forcing of different climate variables, it’s likely to underestimate the change in all-sky SIRF because of the poor representation of sea-ice albedo and cloud–radiation interactions (too much of the surface albedo effect of sea ice is masked by all sky radiative kernels). After correction, the change in all-sky SIRF can be adjusted to 0.33 ± 0.09 W m^{-2}, yield an adjusted SIAF of 0.43 W m^{-2} K^{-1} for the NH and 0.31 W m^{-2} K^{-1} for the entire globe. Three regions: Baffin Bay, North Barents-Kara Sea, and Chukchi Sea, played leading roles in decrease of NH SIRF during the period.

This study also determined both ERA-Interim and MERRA reanalysis products substantially underestimate the change in SIRF due to the poor replication of the change in sea ice albedo in melt season (May to August) and the polar region (north of 80°N). Considering the reports of previous studies (Dessler 2013; Flanner et al. 2011), we conclude that both reanalysis data and GCMs (CMIP3 and CMIP5) underestimate the change in SIRF over the last three decades. To achieve a realistic estimate of sea ice variation, more accurate data simulation and assimilation in melt season and the polar region is needed for reanalysis products.

Acknowledgment: This study is supported by the High-Tech Research and Development Program of China (No.2013AA121201) and the China Scholarship Council. The sea ice extent product was obtained from National Snow and Ice Data Center (NSIDC), the CLARA-A1 data from the Climate Monitoring Satellite Application Facility (CM SAF) project, ERA-Interim data from the European Centre for Medium-Range Weather Forecasts (ECMWF), MERRA albedo product from the NASA's Global Modeling and Assimilation Office, the SSF1deg radiative and cloud products from the NASA Clouds and Earth's Radiant Energy System, the surface temperature from the NASA Goddard Institute for Space Studies. We thank Meredith G. L. Brown for polishing this manuscript. We also wish to thank two anonymous reviewers for their constructive comments, which have greatly improved the presentation of this paper.

References:

Colman, R. A., 2003: A comparison of climate feedbacks in general circulation models. *Climate Dynamics*, **20,** 865-873.

Colman, R. A., 2013: Surface Albedo Feedbacks from climate variability and change. *Journal of Geophysical Research: Atmospheres*, **118,** 2827- 2834.

Comiso, J. C., and D. K. Hall, 2014: Climate trends in the Arctic as observed from space. *Wiley Interdisciplinary Reviews: Climate Change*, **5,** 389-409.

Comiso, J. C., C. L. Parkinson, R. Gersten, and L. Stock, 2008: Accelerated decline in the Arctic sea ice cover. *Geophysical Research Letters*, **35,** L01703.

Crook, J. A., P. M. Forster, and N. Stuber, 2011: Spatial Patterns of Modeled Climate Feedback and Contributions to Temperature Response and Polar Amplification. *Journal of Climate*, **24,** 3575-3592.

Dee, D. P., and Coauthors, 2011: The ERA-Interim reanalysis: configuration and performance of the data assimilation system. *Quarterly Journal of the Royal Meteorological Society*, **137,** 553-597.

Dessler, A., 2013: Observations of Climate Feedbacks over 2000–2010 and Comparisons to Climate Models. *Journal of Climate*, **26,** 333-342.

Dessler, A. E., M. R. Schoeberl, T. Wang, S. M. Davis, and K. H. Rosenlof, 2013: Stratospheric water vapor feedback. *Proceedings of the National Academy of Sciences*, **110,** 18087-18091.

Donohoe, A., and D. S. Battisti, 2011: Atmospheric and Surface Contributions to Planetary Albedo. *Journal of Climate*, **24,** 4402-4418.

Flanner, M. G., K. M. Shell, M. Barlage, D. K. Perovich, and M. A. Tschudi, 2011: Radiative forcing and albedo feedback from the Northern Hemisphere cryosphere between 1979 and 2008. *Nature Geoscience*, **4,** 151-155.

Graversen, R. G., P. L. Langen, and T. Mauritsen, 2014: Polar amplification in the CCSM4 climate model, the contributions from the lapse-rate and the surface-albedo feedbacks. *Journal of Climate*, **27,** 4433-4450.

Hansen, J., R. Ruedy, M. Sato, and K. Lo, 2010: Global Surface Temperature Change. *Reviews of Geophysics*, **48,** RG4004.

Karlsson, J., and G. Svensson, 2013: Consequences of poor representation of Arctic sea-ice albedo and cloud-radiation interactions in the CMIP5 model ensemble. *Geophysical Research Letters*, **40,** 4374-4379.

Karlsson, K. G., and Coauthors, 2013: CLARA-A1: a cloud, albedo, and radiation dataset from 28 yr of global AVHRR data. *Atmospheric Chemistry and Physics*, **13,** 5351-5367.

Kerr, R. A., 2009: Arctic Summer Sea Ice Could Vanish Soon But Not Suddenly. *Science*, **323,** 1655.

Koenigk, T., A. Devasthale, and K. G. Karlsson, 2014: Summer Arctic sea ice albedo in CMIP5 models. *Atmospheric Chemistry and Physics*, **14,** 1987-1998.

Kumar, A., and Coauthors, 2010: Contribution of sea ice loss to Arctic amplification. *Geophysical Research Letters*, **37,** L21701.

Kwok, R., and D. A. Rothrock, 2009: Decline in Arctic sea ice thickness from submarine and ICESat records: 1958-2008. *Geophysical Research Letters*, **36,** L15501.

Markus, T., J. C. Stroeve, and J. Miller, 2009: Recent changes in Arctic sea ice melt onset, freezeup, and melt season length. *Journal of Geophysical Research*, **114,** C12024.

Maslanik, J., C. Fowler, J. Stroeve, S. Drobot, J. Zwally, D. Yi, and W. Emery, 2007: A younger, thinner Arctic ice cover: Increased potential for rapid, extensive sea-ice loss. *Geophysical Research Letters*, **34,** L24501.

Parkinson, C. L., and D. J. Cavalieri, 2012: Antarctic sea ice variability and trends, 1979-2010. *The Cryosphere*, **6,** 871-880.

Perket, J., M. G. Flanner, and J. E. Kay, 2014: Diagnosing shortwave cryosphere radiative effect and its 21st century evolution in CESM. *Journal of Geophysical Research: Atmospheres*, **119,** 1356-1362.

Perovich, D. K., S. V. Nghiem, T. Markus, and A. Schweiger, 2007a: Seasonal evolution and interannual variability of the local solar energy absorbed by the Arctic sea ice–ocean system. *Journal of Geophysical Research*, **112,** C03005.

Perovich, D. K., B. Light, H. Eicken, K. F. Jones, K. Runciman, and S. V. Nghiem, 2007b: Increasing solar heating of the Arctic Ocean and adjacent seas, 1979–2005: Attribution and role in the ice-albedo feedback. *Geophysical Research Letters*, **34,** L19505.

Pistone, K., I. Eisenman, and V. Ramanathan, 2014: Observational determination of albedo decrease caused by vanishing Arctic sea ice. *PNAS*, **11,** 3322-3326.

Pithan, F., and T. Mauritsen, 2014: Arctic amplification dominated by temperature feedbacks in contemporary cliamte models. *Nature Geoscience*, **7,** 181-184.

Qu, X., and A. Hall, 2006: Assessing snow albedo feedback in simulated climate change. *Journal of Climate*, **19,** 2617-2630.

Qu, X., and A. Hall, 2013: On the persistent spread in snow-albedo feedback. *Climate Dynamics*, **42,** 69-81.

Rienecker, M. M., and Coauthors, 2011: MERRA: NASA's Modern-Era Retrospective Analysis for Research and Applications. *Journal of Climate*, **24,** 3624-3648.

Riihelä, A., T. Manninen, and V. Laine, 2013a: Observed changes in the albedo of the Arctic sea-ice zone for the period 1982–2009. *Nature Climate Change*, **3,** 895-898.

Riihelä, A., T. Manninen, V. Laine, K. Andersson, and F. Kaspar, 2013b: CLARA-SAL: a global 28 yr timeseries of Earth's black-sky surface albedo. *Atmospheric Chemistry and Physics*, **13,** 3743-3762.

Screen, J. A., and I. Simmonds, 2010: The central role of diminishing sea ice in recent Arctic temperature amplification. *Nature*, **464,** 1334-1337.

Serreze, M., A. P. Barrett, J. C. Stroeve, D. N. Kindig, and M. M. Holland, 2009: The emergence of surface-based Arctic amplification. *The Cryosphere*, **2,** 601-622.

Serreze, M. C., A. P. Barrett, and J. Stroeve, 2012: Recent changes in tropospheric water vapor over the Arctic as assessed from radiosondes and atmospheric reanalyses. *Journal of Geophysical Research*, **117,** D10104.

Shell, K. M., J. T. Kiehl, and C. A. Shields, 2008: Using the Radiative Kernel Technique to Calculate Climate Feedbacks in NCAR's Community Atmospheric Model. *Journal of Climate*, **21,** 2269-2282.

Soden, B. J., I. M. Held, R. Colman, K. M. Shell, J. T. Kiehl, and C. A. Shields, 2008: Quantifying Climate Feedbacks Using Radiative Kernels. *Journal of Climate*, **21,** 3504-3520.

Stroeve, J., M. M. Holland, W. Meier, T. Scambos, and M. Serreze, 2007: Arctic sea ice decline: Faster than forecast. *Geophysical Research Letters*, **34,** L09501.

Stroeve, J. C., T. Markus, L. Boisvert, J. Miller, and A. Barrett, 2014: Changes in Arctic melt season and implications for sea ice loss. *Geophysical Research Letters*, **41,** 1216-1225.

Taylor, P. C., M. Cai, A. Hu, J. Meehl, W. Washington, and G. J. Zhang, 2013: A Decomposition of Feedback Contributions to Polar Warming Amplification. *Journal of Climate*, **26,** 7023-7043.

Winton, M., 2006: Amplified Arctic climate change: What does surface albedo feedback have to do with it? *Geophysical Research Letters*, **33,** L03701.

Tables

Table 1: Northern Hemisphere (NH) sea ice radiative forcing (SIRF), in W m^{-2}, averaged over 1982–2009 and two kernels' estimates for all three albedo products (CLARA, ERA-Interim, and MERRA). Uncertainties are the 95% confidence intervals of the multi-year averaged SIRFs, Min and Max are the minimum and maximum values of the SIRF time series.

	All-Sky				**Clear-Sky**			
	Mean	Uncertainty	Min	Max	Mean	Uncertainty	Min	Max
CLARA	-1.65	0.14	-1.78	-1.49	-2.95	0.32	-3.26	-2.58
ERA-I	-1.71	0.08	-1.78	-1.63	-3.08	0.17	-3.24	-2.91
MERRA	-1.4	0.07	-1.46	-1.33	-2.62	0.15	-2.77	-2.43

Table 2: Northern Hemisphere (NH) and global sea ice albedo feedback (SIAF), in W m^{-2} K^{-1}. The ranges (Low and High) indicate the extreme minimum/maximum combinations of ΔSIRF and ΔT_s considering the uncertainties of both ΔSIRF and ΔT_s**.**

	NH			**Global**		
	SIAF	Low	High	SIAF	Low	High
CLARA	0.25	0.16	0.40	0.19	0.11	0.30
ERA-I	0.13	0.06	0.22	0.09	0.05	0.17
MERRA	0.10	0.05	0.17	0.07	0.04	0.13

Figure captions

Fig. 1 Seasonal cycles (March to September) of the Northern Hemisphere (NH) sea ice radiative forcing (SIRF) averaged over 1982–2009 and two radiative kernels for all three products for (a) all-sky and (b) clear-sky. The whiskers depict the 95% confidence intervals of the multi-year averaged SIRFs.

Fig. 2 Northern Hemisphere (NH) sea ice radiative forcing (SIRF) averaged over 1982–2009 for (a) CLARA all-sky, (b) CLARA clear-sky, (c) ERA-Interim all-sky, (d) ERA-Interim clear-sky, (e) MERRA all-sky, (f) MERRA clear-sky. SIRFs here are the mean value of estimates with two radiative kernels.

Fig. 3 Northern Hemisphere (NH) sea ice radiative forcing (SIRF) averaged over two radiative kernels and the estimated changes of SIRFs (ΔSIRF) from 1982 to 2009 (W m^{-2}) for (a) all-sky and (b) clear-sky. The 95% confidence intervals of the ΔSIRF were also given. All linear changes have passed the 0.01 significance test.

Fig. 4 Seasonal cycles of Northern Hemisphere (NH) changes in sea ice radiative forcing (ΔSIRF) based on the average of two radiative kernels from 1982 to 2009 for (a) all-sky and (b) clear-sky. The whiskers depict the 95% confidence intervals of monthly changes of SIRFs. All of the changes, except value from ERA-Interim in July (0.1), have passed the 0.05 significance test.

Fig. 5 Changes in sea ice radiative forcing (ΔSIRF) from 1982 to 2009 based on two radiative kernels for (a) CLARA all-sky, (b) CLARA clear-sky, (c) ERA-Interim all-sky, (d) ERA-Interim clear-sky, (e) MERRA all-sky, (f) MERRA clear-sky.

Fig. 6 Annual averaged (January - December) Goddard Institute of Space Studies (GISS) surface temperature anomaly over the Northern Hemisphere (NH, Black) and the entire globe (GL, Blue) from 1982 to 2009. GISS surface temperature anomaly is calculated based on 1951-1980 climatology. The linear changes in surface temperature from 1982 to 2009 and the 95% confidence interval of the changes are given.

Fig. 7 Annual averaged (a) CLARA sea ice radiative forcing (SIRF); (b) Single Satellite Footprint (SSF) top of atmosphere (TOA) upward shortwave (SW) flux; and (c) calculated SSF cloudy-sky SW, adjusted all-sky SW flux, and cloud fraction. Figure 7 (d) is the scatter plot of cloudy-sky upward SW flux and clear-sky upward flux. In subplot (a), (b) and (c), the linear changes of each variable over 2000 to 2009 and the 95% confidence interval of the changes are given. For SSF cloud fraction, the multi-year average and the 95% confidence intervals of the mean value are also given.

Fig. 8 Annual averaged (March - September) CLARA cloud fraction (CFC) over the Northern Hemisphere (NH) sea ice covered region from 1982 to 2009. The linear change in the cloud fraction time series (ΔCFC) from 1982 to 2009 and the 95% confidence intervals of the change are given. The multi-year average of CFC and the 95% confidence intervals of the mean value are also given.

Figures

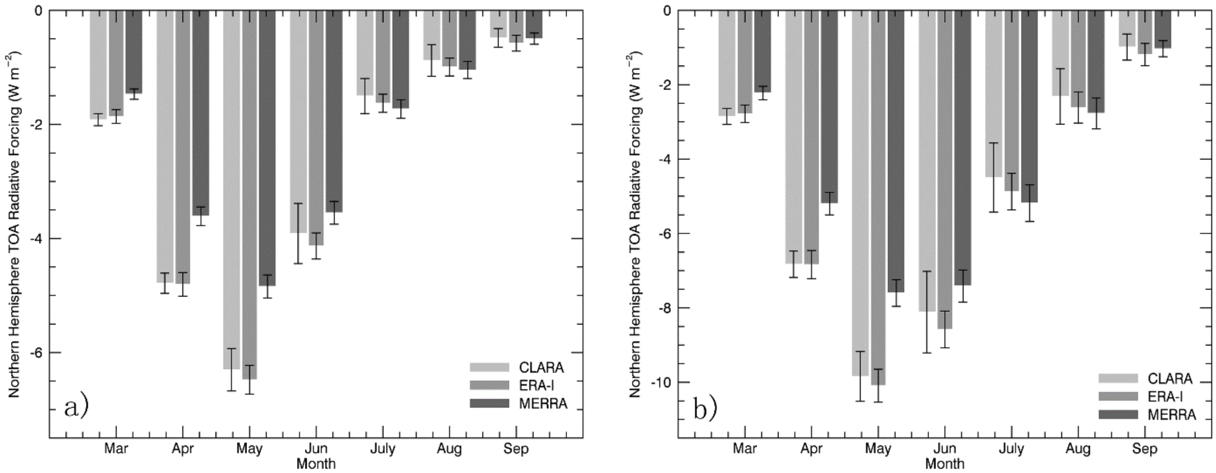

Fig. 1 Seasonal cycles (March to September) of the Northern Hemisphere (NH) sea ice radiative forcing (SIRF) averaged over 1982–2009 and two radiative kernels for all three products for (a) all-sky and (b) clear-sky. The whiskers depict the 95% confidence intervals of the multi-year averaged SIRFs.

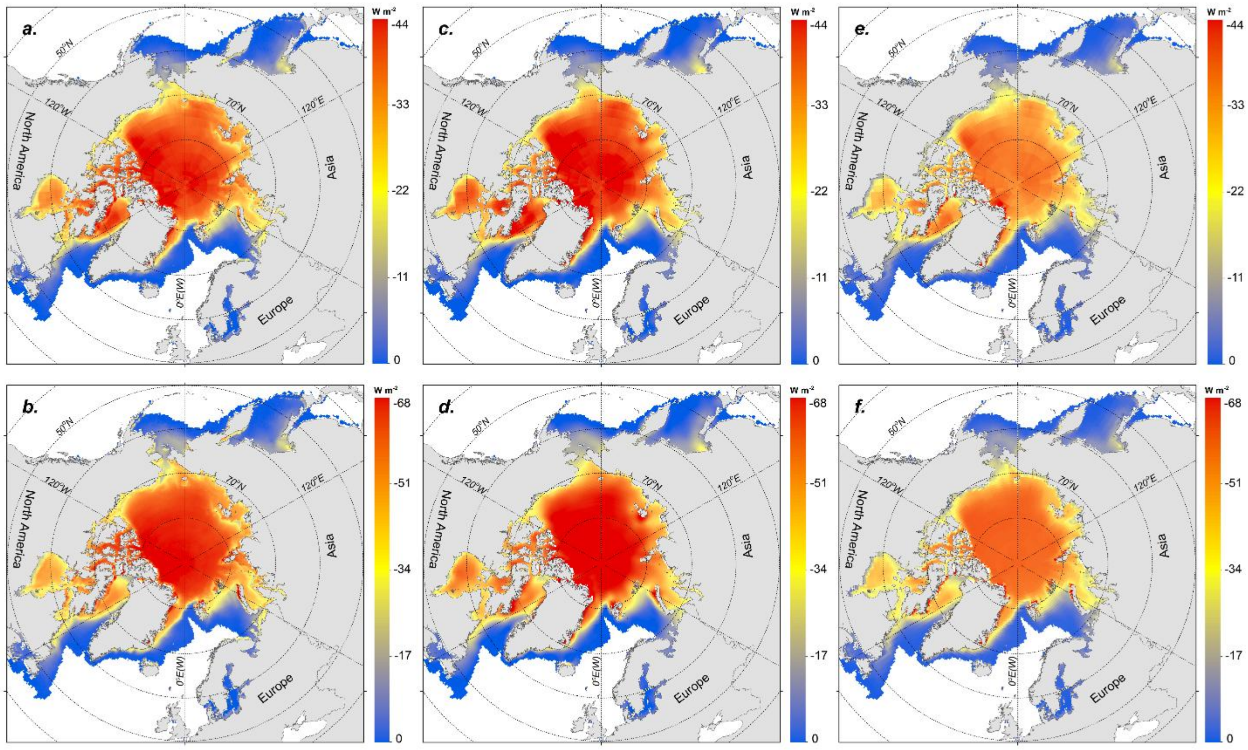

Fig. 2 Northern Hemisphere (NH) sea ice radiative forcing (SIRF) averaged over 1982–2009 for (a) CLARA all-sky, (b) CLARA clear-sky, (c) ERA-Interim all-sky, (d) ERA-Interim clear-sky, (e) MERRA all-sky, (f) MERRA clear-sky. SIRFs here are the mean value of estimates with two radiative kernels.

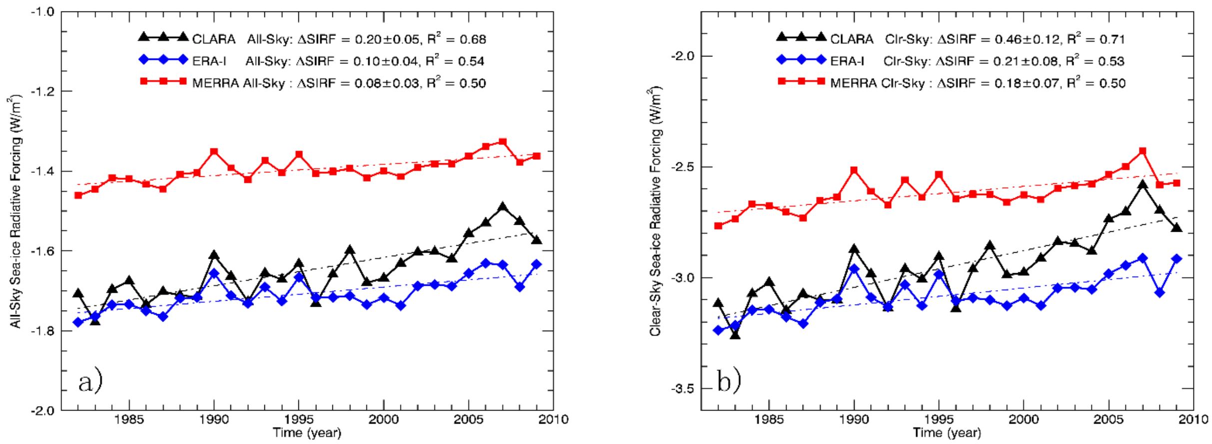

Fig. 3 Northern Hemisphere (NH) sea ice radiative forcing (SIRF) averaged over two radiative kernels and the estimated changes of SIRFs (ΔSIRF) from 1982 to 2009 (W m^{-2}) for (a) all-sky and (b) clear-sky. The 95% confidence intervals of the ΔSIRF were also given. All linear changes have passed the 0.01 significance test.

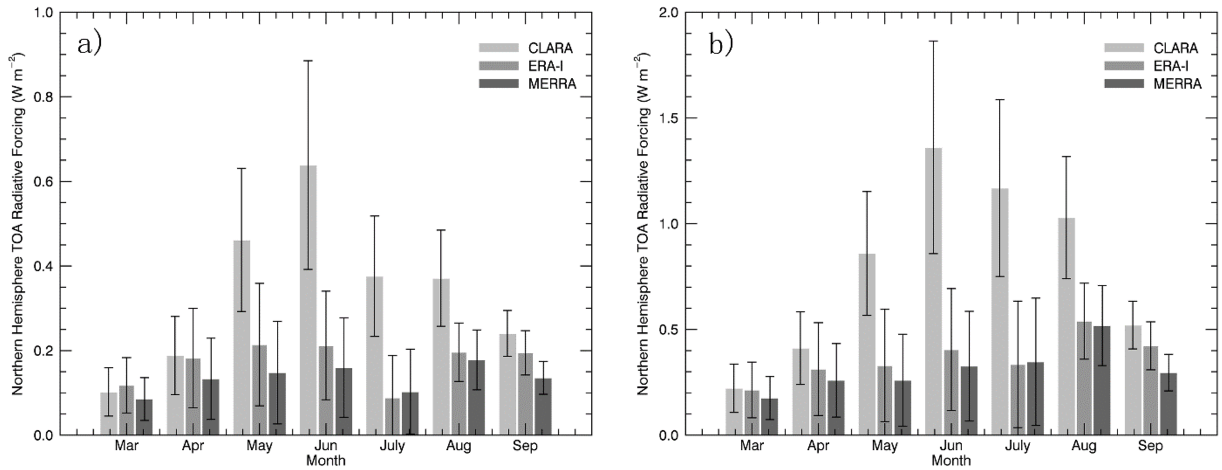

Fig. 4 Seasonal cycles of Northern Hemisphere (NH) changes in sea ice radiative forcing (ΔSIRF) based on the average of two radiative kernels from 1982 to 2009 for (a) all-sky and (b) clear-sky. The whiskers depict the 95% confidence intervals of monthly changes of SIRFs. All of the changes, except value from ERA-Interim in July (0.1), have passed the 0.05 significance test.

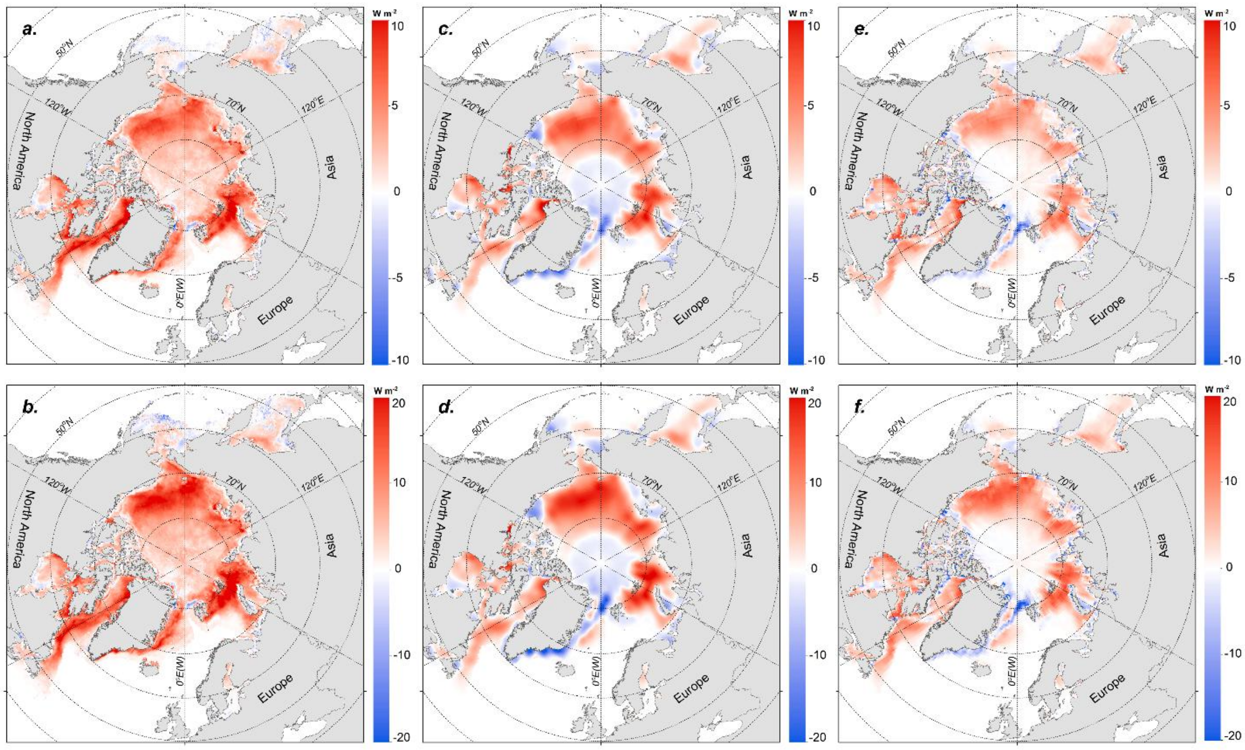

Fig. 5 Changes in sea ice radiative forcing (ΔSIRF) from 1982 to 2009 based on two radiative kernels for (a) CLARA all-sky, (b) CLARA clear-sky, (c) ERA-Interim all-sky, (d) ERA-Interim clear-sky, (e) MERRA all-sky, (f) MERRA clear-sky.

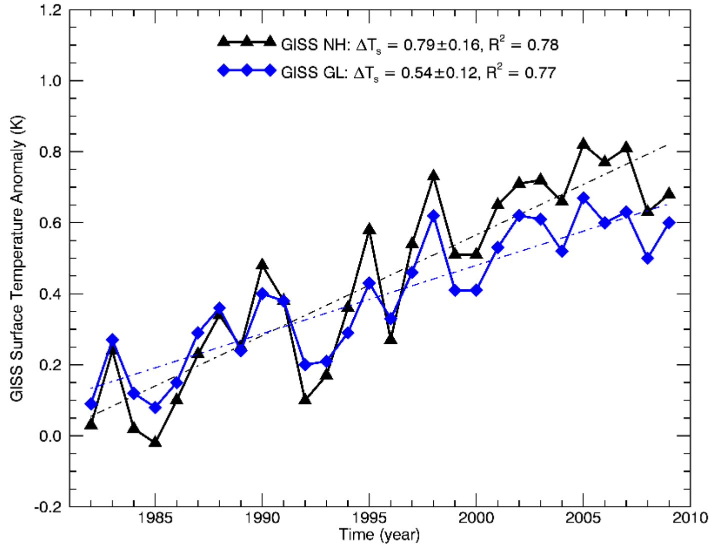

Fig. 6 Annual averaged (January - December) Goddard Institute of Space Studies (GISS) surface temperature anomaly over the Northern Hemisphere (NH, Black) and the entire globe (GL, Blue) from 1982 to 2009. GISS surface temperature anomaly is calculated based on 1951-1980 climatology. The linear changes in surface temperature from 1982 to 2009 and the 95% confidence interval of the changes are given.

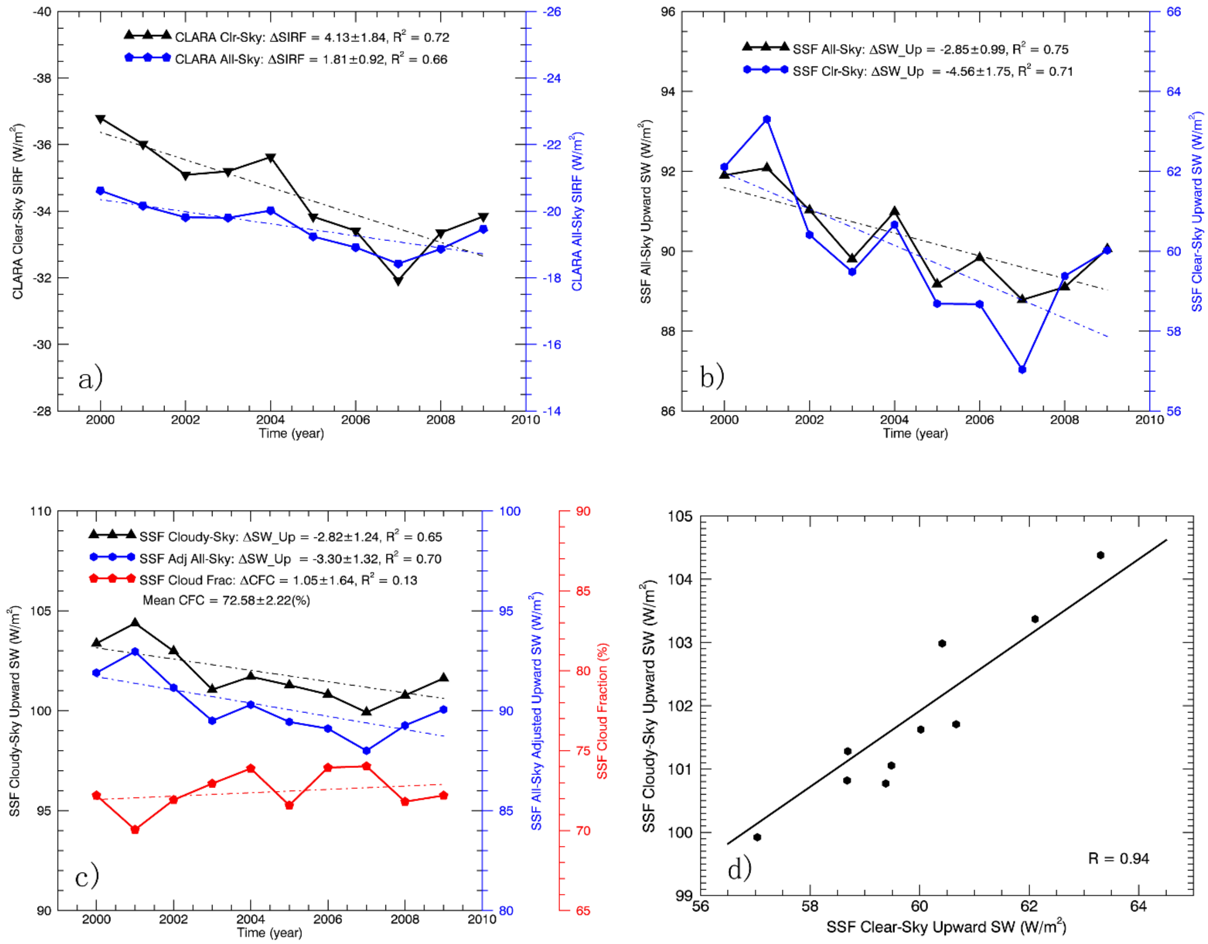

Fig. 7 Annual averaged (a) CLARA sea ice radiative forcing (SIRF); (b) Single Satellite Footprint (SSF) top of atmosphere (TOA) upward shortwave (SW) flux; and (c) calculated SSF cloudy-sky SW, adjusted all-sky SW flux, and cloud fraction. Figure 7 (d) is the scatter plot of cloudy-sky upward SW flux and clear-sky upward flux. In subplot (a), (b) and (c), the linear changes of each variable over 2000 to 2009 and the 95% confidence interval of the changes are given. For SSF cloud fraction, the multi-year average and the 95% confidence intervals of the mean value are also given.

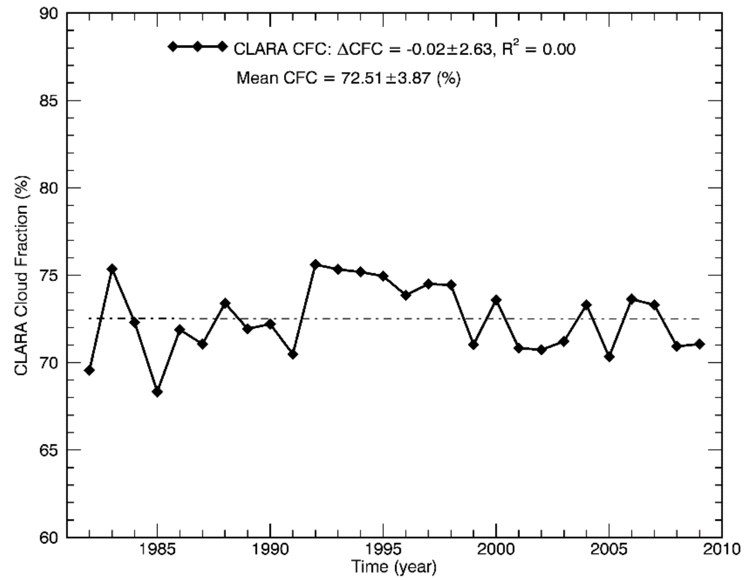

Fig. 8 Annual averaged (March - September) CLARA cloud fraction (CFC) over the Northern Hemisphere (NH) sea ice covered region from 1982 to 2009. The linear change in the cloud fraction time series (ΔCFC) from 1982 to 2009 and the 95% confidence intervals of the change are given. The multi-year average of CFC and the 95% confidence intervals of the mean value are also given.